Catalysis Surveys from Asia (2023) 27:319–331
https://doi.org/10.1007/s10563-023-09402-1

REVIEW

Recent Advances in the Regulation of Oxygen Vacancies in MnO_2 Nanocatalysts

Y. H. Zhou[1] · X. X. Lei[1] · J. Y. Zhou[1] · D. L. Yan[1] · B. Deng[1] · Y. D. Liu[2] · W. L. Xu[1]

Received: 22 February 2023 / Accepted: 27 May 2023 / Published online: 16 June 2023

Abstract
Enhanced oxygen vacancy (V_O) has been designated as an effective strategy to prepare high-performance MnO_2 nanocatalysts for the oxidation of volatile organic compounds (VOC) for thereof unbalanced electronic structure, and rapid electron transfer which may even reduce the reaction temperature down to room temperature. Herein, the effects of the V_O on the catalytic performance of nano-sized MnO_2 were discussed by classifying the V_O into surface-anchored and bulk-involved ones. Currently used introducing and modulating methods for V_O including elemental doping, energetic particle bombardment, atmosphere heat treatment, mechanical chemistry, and redox methods are detailly reviewed. Corresponding regulating mechanisms for V_O are expounded. Commonly used characterization methods including ESR, XPS, HRTEM, and UV-vis are reviewed. Furtherly, the unveiled question which is highly expected to be answered on V_O of MnO_2 nanocatalysts is proposed. The purpose of this review is to present the current status of research on MnO_2 nanoparticles and to provide researchers with basic research ideas.

Keywords Oxygen vacancy · Volatile organic compounds · Manganese dioxide · Low-temperature catalytic oxidation · Heterogeneous catalysis

1 Introduction

In recent years, with the boosted industrialization, the environmental pollution caused by volatile organic pollutant (VOC) emissions has attracted widespread attention [1]. To solve the VOC environmental pollution, among many efficient green catalytic technologies, nanocatalysts are highly promising due to their high response rate, high catalytic activity, and large specific surface area [2].

As a new inorganic catalytic material, MnO_2 nanoparticles stand out from other nano-catalytic materials based on the following points.

(1) Its ability to respond to both light and heat and its ability to catalyse the degradation of organic pollutants at room temperature or in the absence of light, allowing for a wider range of applications [3].
(2) The wide range of crystalline forms (Fig. 1), can be adjusted by hydrothermal synthesis and high-temperature treatment to modulate their catalytic performance for different pollutants.
(3) Among all the transition metal oxides, MnO_2 has the highest catalytic activity for formaldehyde [4].
(4) It has the advantages of high activity, low toxicity, low cost, and abundant raw material reserves.

In addition to the selective modulation of MnO_2 crystalline form, the temperature, precursor concentration, and precursor type can also be regulated to fabricate MnO_2 catalysts with different morphologies such as nanorods, nanowires, and nanoflowers, enabling MnO_2 catalysts with superior

✉ B. Deng
dengjianguo88@outlook.com

✉ Y. D. Liu
liuyd@sxicc.ac.cn

✉ W. L. Xu
weilin-xu@hotmail.com

[1] State Key Laboratory of New Textile Materials & Advanced Processing Technologies and Hubei Key Laboratory of Advanced Textile Materials & Application, Wuhan Textile University, Wuhan 430200, Hubei, China

[2] Institute of Coal Chemistry, Chinese Academy of Sciences, Taiyuan 030000, Shanxi, China

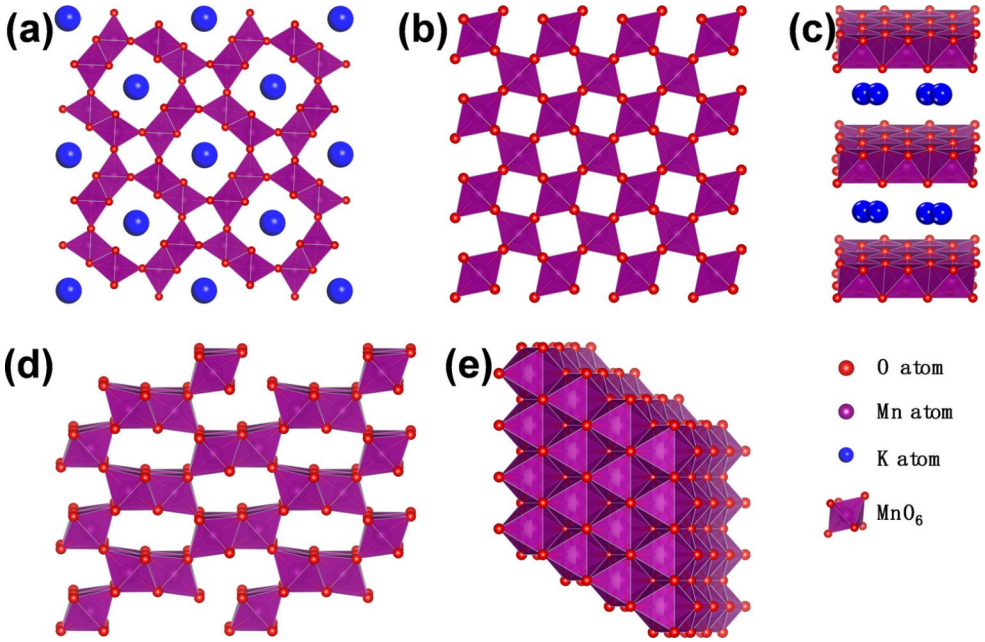

Fig. 1 MnO_2 catalysts of various crystal types [5] (**a**) α-MnO_2, (**b**) β-MnO_2, (**c**) δ-MnO_2, (**d**) γ-MnO_2, and (**e**) ε-MnO_2.

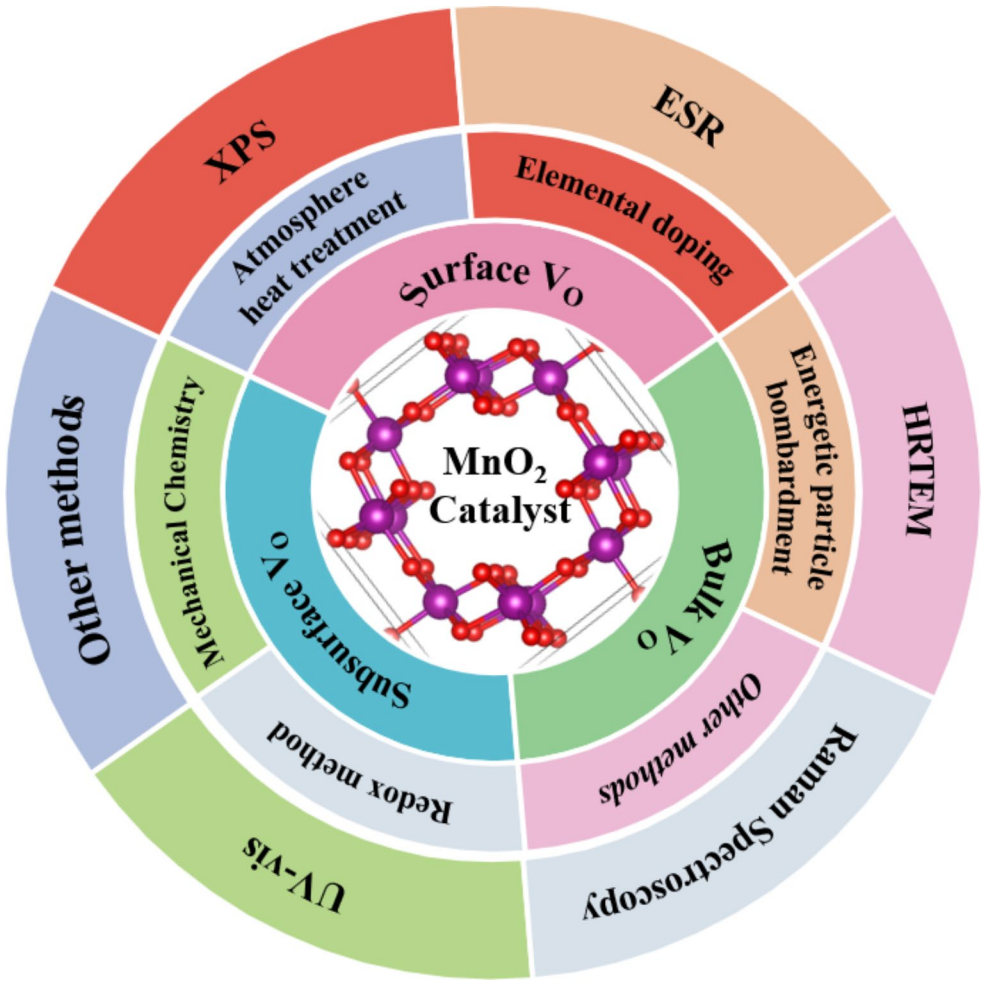

Fig. 2 Classification, introducing and modulating, and characterization methods of Vo for MnO_2 nano-catalyst

catalytic performance. Wang et al. prepared nano-α-MnO_2 in the form of rods, wires, and tubes, respectively, and found that the rod-shaped α-MnO_2 had the best catalytic degradation performance for formaldehyde [6].

However, the nano-MnO_2 catalysts also suffer from high photogenerated electron-hole complexation rates and low catalytic activity at low temperatures [7]. To solve these problems, researchers have tried many methods, such as elemental doping, heterostructure construction, defect engineering [8] (crystal plane control, V_O), etc. All existing studies have found that oxygen vacancies act as adsorption and active sites that can capture gaseous oxygen and activate it into active oxygen species thus improving the catalytic activity of MnO_2 [9]. A detailed review of the modulation mechanism of oxygen vacancies in MnO_2 nanoparticles and their effects on the catalytic activity has not been reported. Therefore, this paper presents a review of the recent research progress on the effects of oxygen vacancies (V_O) on the catalytic activity of MnO_2, the introduction and modulation of V_O, and the characterization method of V_O as shown in Fig. 2.

2 Effects of The V_O on The Catalytic Performance of Nano-sized MnO_2

2.1 The Definition of V_O

The term, V_O, was first introduced by scientists in 1960. The oxygen-deficient vacancies formed by the escape of lattice oxygen in metal oxides are known as V_O (oxygen defects), which are anionic defects and a type of crystal defect (Fig. 3) [7].

The formation of V_O in MnO_2 due to the charge compensation mechanism causes a varied valence state of partial cations to maintain the charge conservation of the catalyst as shown in Eq. (1) [10].

$$2Mn^{4+} + 2O^{2-} + 2Mn^{4+} \rightarrow 2Mn^{3+} + 2V_O + 2Mn^{3+} + O_2 \uparrow \quad (1)$$

According to the location of V_O generated in the catalyst, V_O can be classified as a surface vacancy, subsurface vacancy, and bulk phase oxygen vacancy [11].

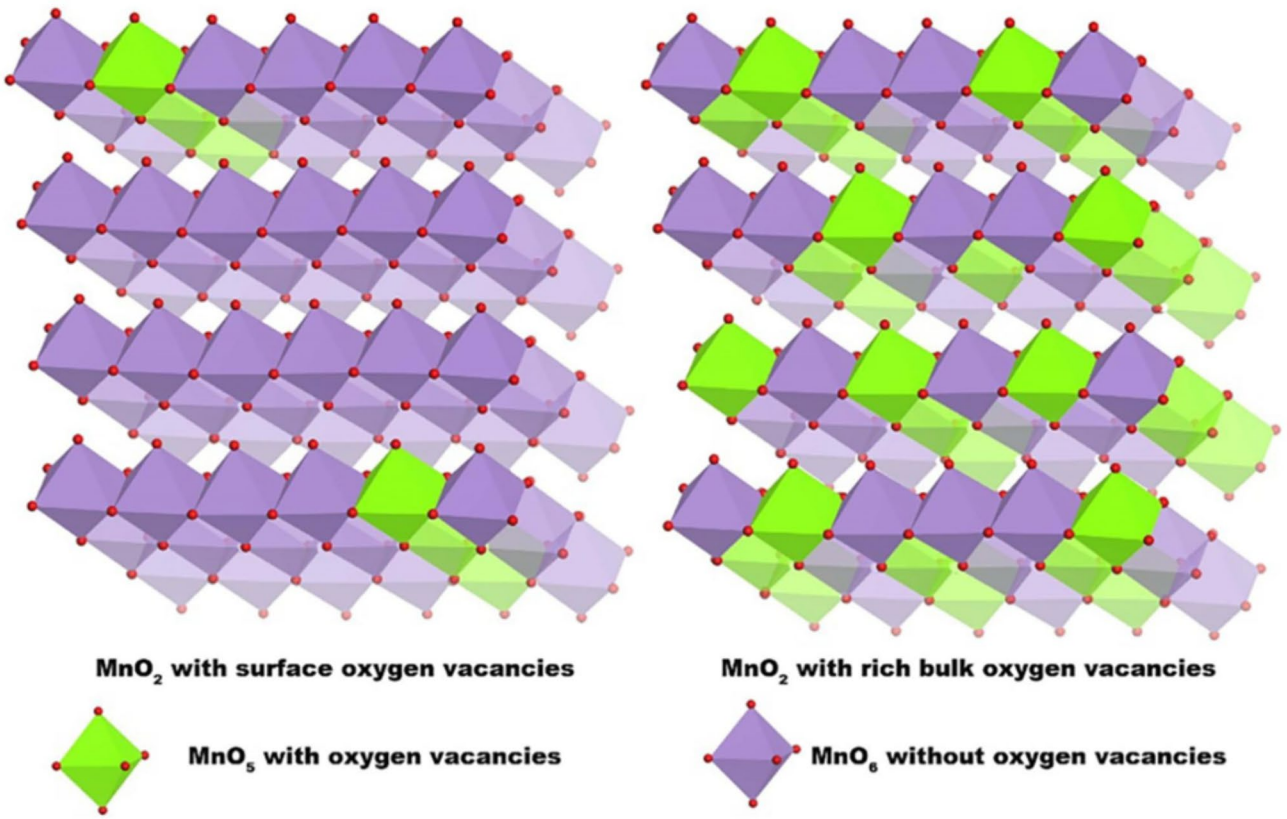

Fig. 3 Bulk-phase and surface V_O in δ-MnO_2 [7]

2.2 Effect of V_O on The Catalytic Performance of MnO_2

It was found that the formation of Mn^{3+}, due to the Jahn-Teller effect, stretches the bond length of Mn-O and makes it easier to break, thus allowing the escape of oxygen atoms [12]. The surface V_O, the bulk phase V_O, and thereof concentrations of MnO_2 affect the catalytic performance of MnO_2 catalysts together. Therefore, we will elaborate on the mechanisms of these three factors on the catalytic performance of MnO_2 individually.

2.2.1 Effect of Surface V_O on The Catalytic Performance of MnO_2

It was found that surface V_O can act as active sites for catalytic reactions and adsorption sites for oxygen [13] and can activate oxygen (O_2) to reactive oxygen species, a process that is a key step in the catalytic oxidation of MnO_2 [14].

The effect of surface V_O on the catalytic performance of MnO_2 is not only an active site's catalytic reaction but also improves the catalytic activity of MnO_2 by promoting the reactivity and mobility of surface lattice oxygen [10]. Santos et al. demonstrated that lattice oxygen can participate in catalytic reactions and partial MnO_2 is reduced to Mn_2O_3 or Mn_3O_4 which could be finally reverted to MnO_2 by filling with oxygen [15]. Zhu et al. proved that the MnO_2 surface V_O affects the lattice oxygen mobility by unbalancing the surface lattice oxygen to allow the escape of V_O close to the surface [8]. Consumed lattice oxygen in the catalytic oxidation reaction can be replenished by adsorbing gaseous oxygen onto the V_O [16].

The mechanism by which surface V_O affects the catalytic performance of MnO_2 is shown in Fig. 4. It is noteworthy that it has not been concluded whether the lattice oxygen participates in the catalytic reaction through V_O after being oxidized to reactive oxygen species or through other forms.

In addition, Cheng et al. showed by density flooding theory (DFT) calculations that surface V_O can reduce the kinetic potential barrier for oxygen reduction reaction (ORR). The kinetic potential barrier is reduced by 0.96 and 0.55 eV after the introduction of 1 to 2 oxygen vacancies on the surface, respectively [17]. Similarly, Yang et al. suggested that V_O can reduce the energy potential barrier for NO reduction and improve the adsorption capacity of the catalyst. Oxygen vacancies reduce the energy barrier for *NH2 formation by more than 0.3 eV as confirmed by NH_3-TPD [18]. Wang et al., suggested that positively charged surface V_O can accumulate free electrons, endowing MnO_2 with a similar role to that of noble metal catalysts [19].

However, some researchers have other views. Wang et al. argued that the oxygen species (i.e., O^{2-}, O_2^{2-}, etc.) or lattice oxygen is the active center of the catalytic reaction [20]. Zhao et al. argued that in the hydrogen precipitation (HER) and oxygen precipitation (OER) reactions, Mn^{3+} acts as the active site, and the V_O promotes H_2O adsorption [9]. Therefore, it is debatable about the active center of MnO_2-catalyzed reactions. Zhu et al. suggested that both surface V_O and cations associated with V_O synergistically affect the catalytic performance of MnO_2 [21].

Some researchers claimed that the MnO_2 surface V_O is unstable. Li et al. suggested that the V_O on the β-MnO_2 surface is occupied by oxygen atoms released during the oxygen reduction reaction (ORR) [11]. Santos suggested that some intermediates of catalytic degradation accumulate and occupy the surface V_O [15]. In a word, the stability of V_O on the MnO_2 surface can be affected by various reaction environments.

2.2.2 Effect of Bulk-phase V_O on The Catalytic Performance of MnO_2

As we all know, MnO_2 is a catalyst of photothermal catalyst. The absorbance of the photo is significant in increasing the performance of the catalyst. The narrowing of the

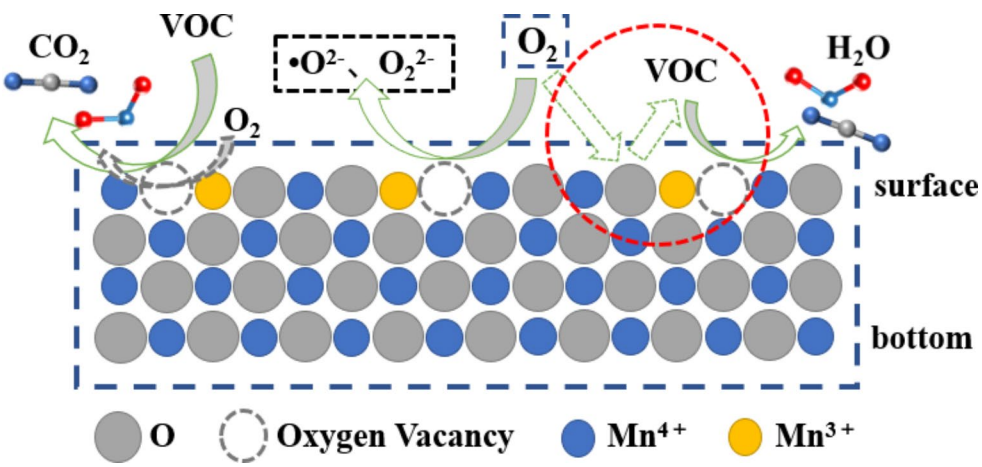

Fig. 4 Mechanism of surface V_O affecting the catalytic performance of MnO_2(side view)

forbidden band width can promote the absorption of light and thus increase the concentration of photogenerated carriers. However, too small a band gap will reduce the redox ability of photogenerated carriers, thus reducing or even losing the photocatalytic ability of MnO_2. Therefore, the effect of the regulation of the MnO_2 band gap on its catalytic performance is also very important. Li et al. found that moderate bulk phase V_O concentration can reduce the band gap of MnO_2 and improve its conductivity through simulations. However, high V_O concentration broadens the band gap and affects its conductivity, and V_O can form new crystalline phases in β-MnO_2 [11]. Zhang et al., calculated by density flooding theory (DFT) that bulk-phase V_O can reduce the band gap of MnO_2, accelerate the electron transfer rate and obtain electron leaving domains [7]. And due to the limitation of objective preparation methods, it is not possible to produce oxygen vacancies only in the bulk phase and not on the surface, so there are fewer studies on the bulk phase oxygen vacancies.

2.2.3 Effect of The Concentration of V_O on The Catalytic Performance of MnO_2

No matter whether for bulk V_O or surface V_O, it's not that the higher the concentration, the better the catalytic performance of MnO_2. The relationship between the electronic structure and catalytic activity of β-MnO_2 in the oxygen reduction reaction (ORR) and the concentration of V_O in the bulk phase was determined by Li et al. [11] Mn_2O_3 is formed when the V_O concentration is too high, and the catalytic performance of Mn_2O_3 is lower than all MnO_2 catalysts generated by the pyrolysis of Mn $(NO_3)_2$, [22] which is not favorable for the oxygen reduction reaction (ORR). However, Wang et al. found that the order of catalytic degradation activity of MnO_2, Mn_2O_3, and Mn_3O_4 for phenol was $Mn_2O_3 > Mn_3O_4 > MnO_2$. They concluded that the catalytic activity of manganese-based oxides is related to oxidation valence and oxygen mobility [23]. Therefore, there is still a debate about the relative strength of the catalytic activity of Mn_2O_3 and MnO_2.

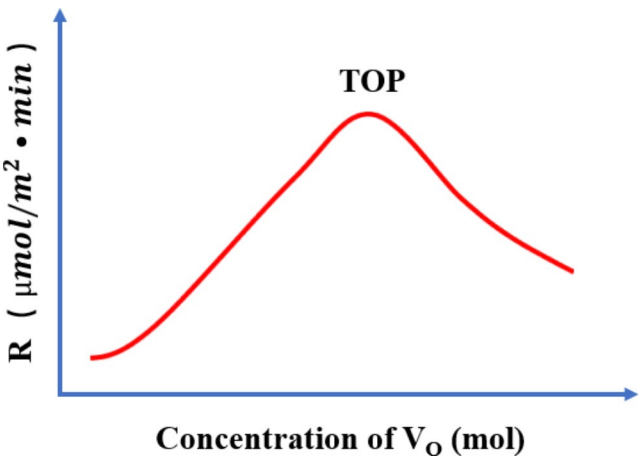

Fig. 5 Relationship between catalyst specific rate and oxygen vacancy content

Qu et al. [16] confirmed, for example, by programmed temperature rise reduction of H_2 (H_2-TPR), that in δ-MnO_2, too high surface V_O concentrations reduce the reduction and mobility of oxygen species in the catalyst, as well as the reduction of Mn^{3+}, to the detriment of the oxidation of toluene. Therefore, in the catalytic degradation of VOC, the effect of oxygen vacancy concentration on the catalytic performance of MnO_2 is shown in Fig. 5. MnO_2 photocatalytic performance is evaluated by detecting the change of VOC and CO_2 content at a certain time under a certain intensity of light.The thermocatalytic performance of VOC at 30 °C is generally evaluated by a fixed reaction bed and Eq. (2)."

$$R(\mu mol/m^2 \bullet min) = \frac{C_{VOC} \div 22.4 \times F \times \eta}{S_{BET} \times m} \times 10^{-5} \quad (2)$$

where R is the specific rate, C_{VOC} is the inlet VOC concentration (ppm), F is the flow rate (mL/min), η is the VOC conversion calculated from CO_2 generation (%), S_{BET} is the sample-specific surface area, and m is the sample weight.

3 The Introduction and Regulation Method of MnO_2 V_O

V_O, as an intrinsic defect, is often present already during the preparation of the catalyst at low concentrations. The catalytic performance of MnO_2 can be enhanced by up-regulating the V_O concentration. Therefore, the desire to obtain MnO_2 catalysts with a suitable concentration of V_O requires artificial introduction and modulation. The following methods for the regulation and introduction of MnO_2 V_O have been reported in the literature.

3.1 Elemental Doping

Elemental doping refers to the introduction of other elements into MnO_2 crystals by physical or chemical methods. From the type of doped elements, it can be divided into metal ion doping and non-metal ion doping. From the doping position, it can be divided into substitution doping and interstitial doping. The V_O concentration can be effectively controlled by controlling the molar ratio of doping elements to Mn elements to introduce V_O.

The doped metal cation is generally used to replace Mn^{4+} in MnO_2, whose valence state is generally smaller than Mn^{4+}. Wang et al. introduced V_O in MnO_2 by replacing

Mn^{4+} in the MnO_2 lattice with Fe^{3+} and Mn^{3+} by a "redox precipitation" method [19]. In addition, Ye et al. prepared Fe, V, and Co-doped MnO_2 electrode materials with good electrical conductivity by electrodeposition, [33] which enhanced the electrocatalytic performance of MnO_2 electrode materials. However, it has not been verified whether the co-doping of multi-metal ions can make MnO_2 obtain more excellent chemical catalytic properties than the single-metal-doped MnO_2.

Non-metallic element doping usually replaces the oxygen element in MnO_2. Chu et al. concluded by DFT calculations that boron doping results in the formation of V_O near the oxygen ions replaced by boron ions in MnO_2, which facilitates the formation of a more stable thermodynamic structure [34]. He et al. obtained N-element substituted and interstitially doped MnO_2 samples by N_2-plasma treatment at different times, and they found that the interstitial doping of N elements can reduce the formation energy of V_O and is more favourable to the formation of V_O [35]. However, the characterization of interstitial N doping needs further improvement. Doping of other non-metallic elements such as F has not been reported.

Some doping elements did not enter the lattice gap or replace Mn^{4+} but replaced K^+ in the MnO_2 tunnel or interlayer to form V_O [36]. Qu et al. introduced V_O in MnO_2 by replacing K^+ in the δ- MnO_2 interlayer with Cu^{2+} and proposed a mechanism for the formation of the corresponding V_O [16].

3.2 Energetic Particle Bombardment

V_O can also be created by breaking the metal-oxygen bonds on the surface of metal oxides through bombardment with high-energy particles (protons, ions, and electrons) and detaching the surface lattice oxygen. By controlling the timing and power of the energetic particle bombardment, the number of V_O introduced can be controlled. The method is more commonly used in metal oxides such as TiO_2 and less commonly reported for MnO_2.

Baeck et al. introduced V_O on the surface of MnO_2 by irradiating it with a high-energy proton beam. The principle is that the water molecules in the air are ionized and decomposed by proton beam irradiation, forming highly reactive radicals. Such radicals further break the Mn-O bond in MnO_2, causing the oxygen element to break away from the lattice and form V_O [37]. However, this method introduces an uncontrollable number of V_O, has high energy consumption, and is not of practical application.

V_O can also be created by breaking the metal-oxygen bonds on the surface of metal oxides through bombardment with high-energy particles (protons, ions, electrons) and detaching the surface lattice oxygen. Baeck et al. introduced a large number of V_O on the surface of MnO_2 by irradiating it with a high-energy proton beam. The principle is that the water molecules in the air are ionized and decomposed by proton beam irradiation, forming highly reactive radicals. Such radicals further break the Mn-O bond in MnO_2, causing the oxygen element to break away from the lattice and form V_O [37]. However, this method introduces an uncontrollable number of V_O, has high energy consumption, and is not of practical application.

3.3 Atmosphere Heat Treatment

Heat treatment in inert or reducing atmospheres, high temperatures can cause lattice oxygen to escape, thus introducing V_O on the MnO_2 surface and subsurface [38]. At high temperatures, oxygen usually refills the V_O to make them burst, so commonly used atmospheres are nitrogen, argon, hydrogen, etc. The concentration of V_O can be regulated by controlling the temperature and time of deoxygenation.

Zhu et al. introduced V_O on the surface of α-MnO_2 nanowires by vacuum deoxygenation at a high temperature, and the concentration of V_O could be adjusted by the temperature and time of deoxygenation [8]. β- MnO_2 nanosheets with abundant V_O were obtained by calcining γ- MnO_2 in the air to cause its phase transformation by Yang et al. [18] The introduction of V_O by atmospheric heat treatment is energy-intensive, the treatment process is complicated, and mass production is not possible.

3.4 Mechanical Chemistry

Mechanochemistry is a method of introducing V_O on MnO_2 by ball milling. During ball milling, friction, and collisions between the spheres and the MnO_2 catalyst break the Mn-O bond on the surface of the latter. Subsequently, V_O is formed by the escape of oxygen from the surface lattice. The content of V_O on the MnO_2 surface can be easily regulated by controlling the time and speed of ball milling [21].

Yang et al. successfully introduced V_O on the MnO_2 surface using ball milling and the modified MnO_2 catalyst had high catalytic activity for VOC [10]. The ball milling method is simple, inexpensive, and solvent-free, and can be supplemented with moderate pressure and temperature regulation to increase the efficiency of V_O generation [39].

3.5 Redox Method

It has been studied that V_O, as an intrinsic defect, is widely distributed in metal oxides [40]. The ultra-thin structured MnO_2 nanosheets, which are usually formed under hydrothermal conditions, possess certain V_O [9].

The production of Mn^{3+} on the surface of MnO_2 catalysts facilitates the formation of V_O. The chemical reaction method regulates the content of Mn^{3+} by adding weak reducing reagents such as ammonia and ammonium chloride to the MnO_2 precursor so that the prepared MnO_2 catalysts have more abundant V_O.

The degree of the redox reaction is changed by adjusting different molar ratios of the reactants to achieve the introduction of oxygen vacancies. The method allows the introduction of V_O in both the surface and bulk phases.

Huang et al. successfully prepared δ-MnO_x loaded on activated carbon using a mixture of ammonia and potassium permanganate, which has excellent degradation performance for formaldehyde at room temperature [41]. Yan et al. introduced V_O on δ- MnO_2 using the reducing ability of NaBH4 and the oxidizing ability of H_2O_2, respectively,[42] and proposed a redox mechanism.

Notably, surface V_O is not only formed on MnO_2 by adding weak reducing agents. Liu et al. prepared nanocarbon-modified δ-MnO_2 nanoflowers with high manganese vacancy (V_{Mn}) content by a one-step hydrothermal method using a redox reaction of glucose or sucrose with potassium permanganate [43]. Zhang et al. in the presence of sodium citrate by a simple generation process δ-MnO_2 nanosheets with abundant bulk-phase V_O were prepared [7].

3.6 Other Methods

In addition to the above common methods, other methods such as hydrothermal (crystal growth), ultrasonic, and plasma treatments have also been used to introduce V_O on MnO_2.

Chen et al. obtained α-MnO_2 with abundant V_O by adjusting the precipitation temperature. Fast-growing crystals are more prone to form crystal defects, and thus V_O on MnO_2 [12]. Cui et al. disrupted the chemical bonding on the surface of α-MnO_2 by the surface erosion of ultrasonic treatment making it easier for lattice oxygen to be released to form V_O [44]. Cai et al. used different times of hydrogen plasma (H-plasma) treatment of δ-MnO_2 to introduce surface V_O. The V_O can be partially refilled by subsequent treatment with oxygen plasma (O-plasma) after the introduction of V_O [45]. This experimental phenomenon indirectly proves the existence of V_O.

The AOS and complete degradation temperature of HCHO via different fabrication methods were summarized in Fig. 6.

4 Common Characterization Methods for V_O

4.1 Quantitative Characterization Method of MnO_2 V_O

4.1.1 X-ray Photoelectron Spectroscopy (XPS)

XPS analysis is commonly used to study the ratio of surface elements in different chemical valence states of catalysts and therefore can also be used to assess the concentration of surface V_O on the MnO_2 surface [49]. The spontaneous charge balance makes the production of V_O usually accompanied by the reduction of a certain chemical equivalent of Mn^{4+} to Mn^{3+}. Therefore, the surface V_O concentration can usually be evaluated in terms of the Mn^{3+} content. The two

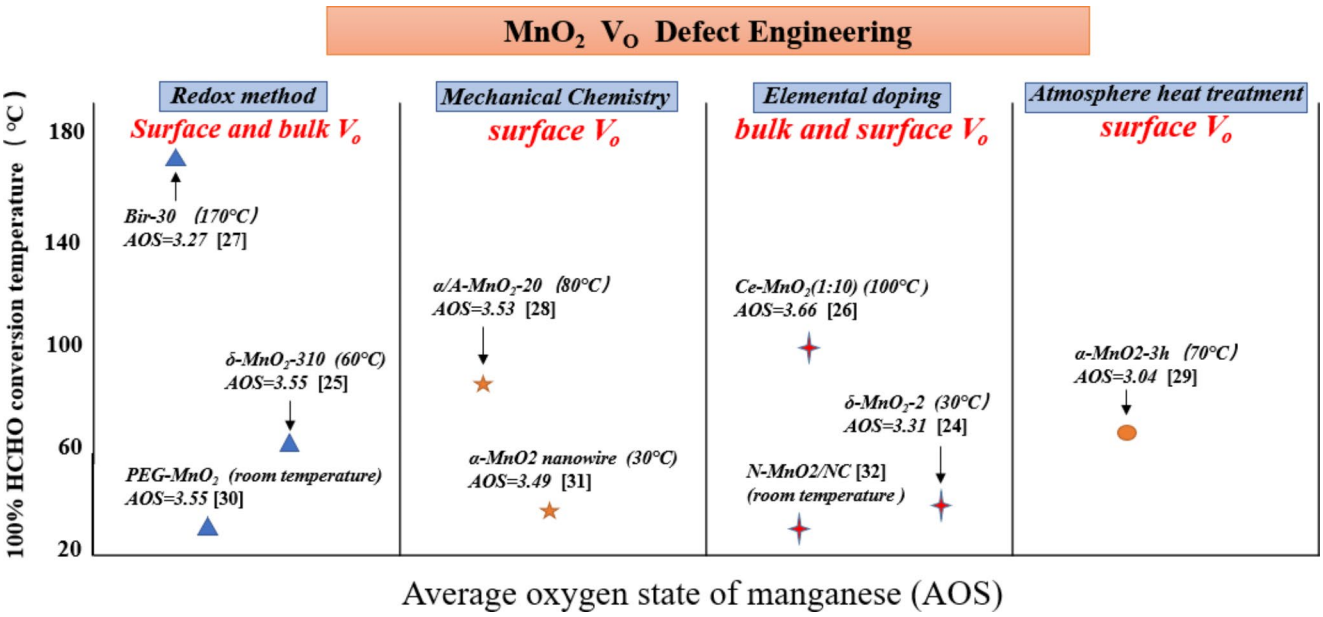

Fig. 6 Summary of the activity of various catalysts prepared using the above strategies at the complete degradation temperature of HCHO [24–32]

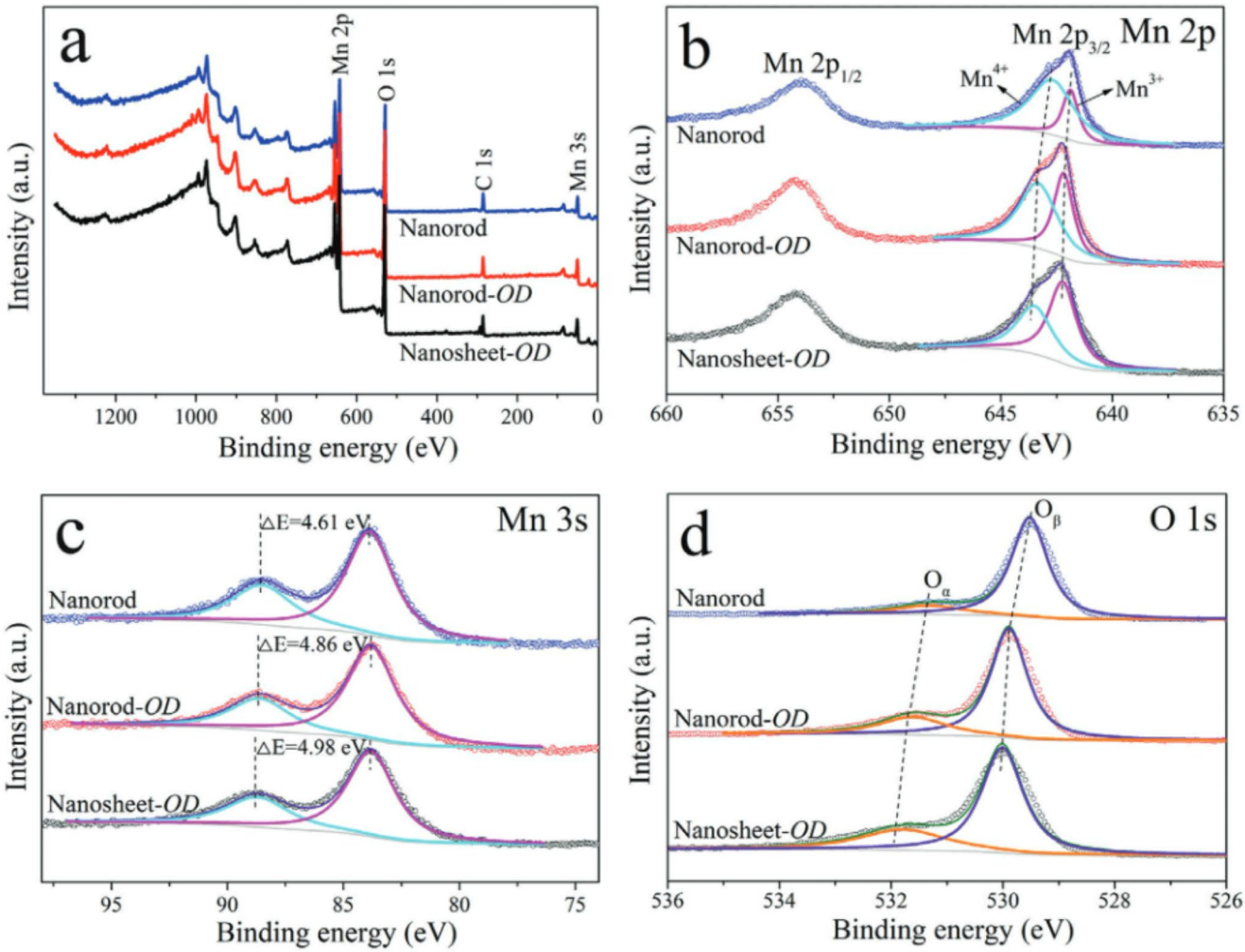

Fig. 7 The XPS spectra of MnO_2 Nanorod and MnO_2 nanorods with V_O (Nanorod-OD) and MnO_2 nanosheets with V_O (Nanosheet-OD) (**a**) survey spectra, (**b**) Mn 2p, (**c**) Mn 3s, (**d**) O 1s

Table 1 Content and ratio of each element on the surface of MnO_2 [53]

Sample	Binding energy (eV)			
	Mn^{3+}	Mn^{4+}	Surface adsorption of oxygen.	Surface lattice oxygen
Nanorod [a]	641.9	642.7	531.3	529.5
Nanorod-OD [b]	643.4	643.4	531.7	529.9
Nanosheet-OD [c]	643.5	643.5	531.9	530.3

[a] MnO_2 Nanorod

[b] MnO_2 nanorods with V_O

[c] MnO_2 nanosheets with V_O

components at 641.9-642.2 eV and 642.7-643.5 eV correspond to Mn^{3+} and Mn^{4+}, respectively, by fitting the split peaks of Mn $2p_{3/2}$, [50] as shown in Fig. 7 [18].

The relative content of Mn^{3+} on the surface of MnO_2 can be calculated by integrating the peak area after splitting peak fitting (Table 1). In addition, the average oxidation state (AOS) of surface Mn can also be calculated by the empirical formula, AOS = 8.956–1.126 × ΔE, ΔE being the splitting width of Mn3s, [51] with smaller AOS values representing higher Mn^{3+} content and higher concentrations of surface V_O.

Finally, the concentration of surface V_O can also be assessed by the content of surface adsorbed oxygen species, since V_O acts as active sites to promote oxygen adsorption and activation, [18] with peaks at 529.5–530.0 eV attributed to lattice oxygen and 531.4-531.8 eV to surface adsorbed oxygen [52].

However, the penetration depth of XPS is usually within 10 nm, [50] which is only applicable to the characterization of surface V_O. For the characterization of V_O in MnO_2 catalysts with larger particle sizes, the ESR method is more suitable.

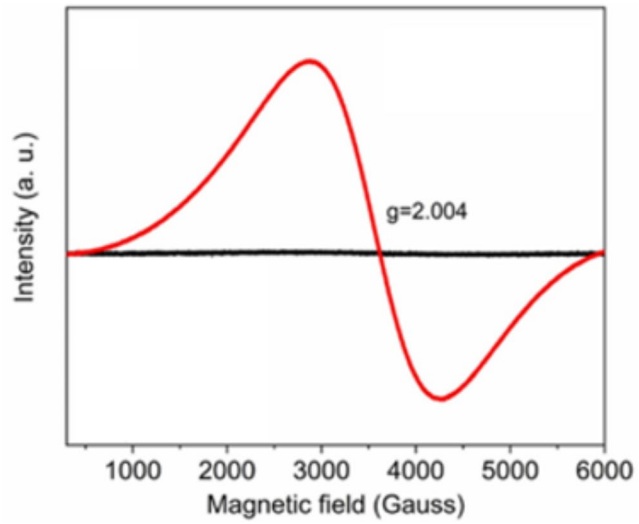

Fig. 8 ESR spectra of MnO_2 V_O

4.1.2 Electron Paramagnetic Resonance (ESR) Method

Electron paramagnetic resonance (ESR) can quantitatively assess the concentration of V_O in catalysts (Fig. 8a) [46]. g value of MnO_2 V_O is about 2.00, [47] the ESR signal is caused by the paramagnetic signal generated by unpaired electrons in MnO_2, [48] and the intensity of the ESR signal (spins/g) is linearly and positively correlated with the concentration of V_O [7]. ESR can be used to characterize both surface and bulk phase V_O.

4.2 Qualitative Characterization Method of MnO_2 V_O

4.2.1 High-resolution Transmission Electron Microscopy (HRTEM)

High-resolution transmission electron microscopy allows the qualitative characterization of surface oxygen vacancies in MnO_2 (Fig. 9a). some of the lattice stripes on the δ-MnO_2 (100) crystal plane become disordered and blurred, possibly due to the formation of surface V_O defects [16]. However, this method needs to be assisted by other characterization methods to further confirm the presence of V_O.

4.2.2 Raman Spectroscopy

Raman spectra can reflect the structural information of the samples, and with the increase of V_O concentration, the summits at ≈500 and ≈630–650 cm^{-1} of the Raman spectra of MnO_2 undergo a significant blue shift, indicating the enhancement of Mn-O vibrations in the [MnO_6] group, which is due to the lattice distortion caused by V_O (Fig. 9b)

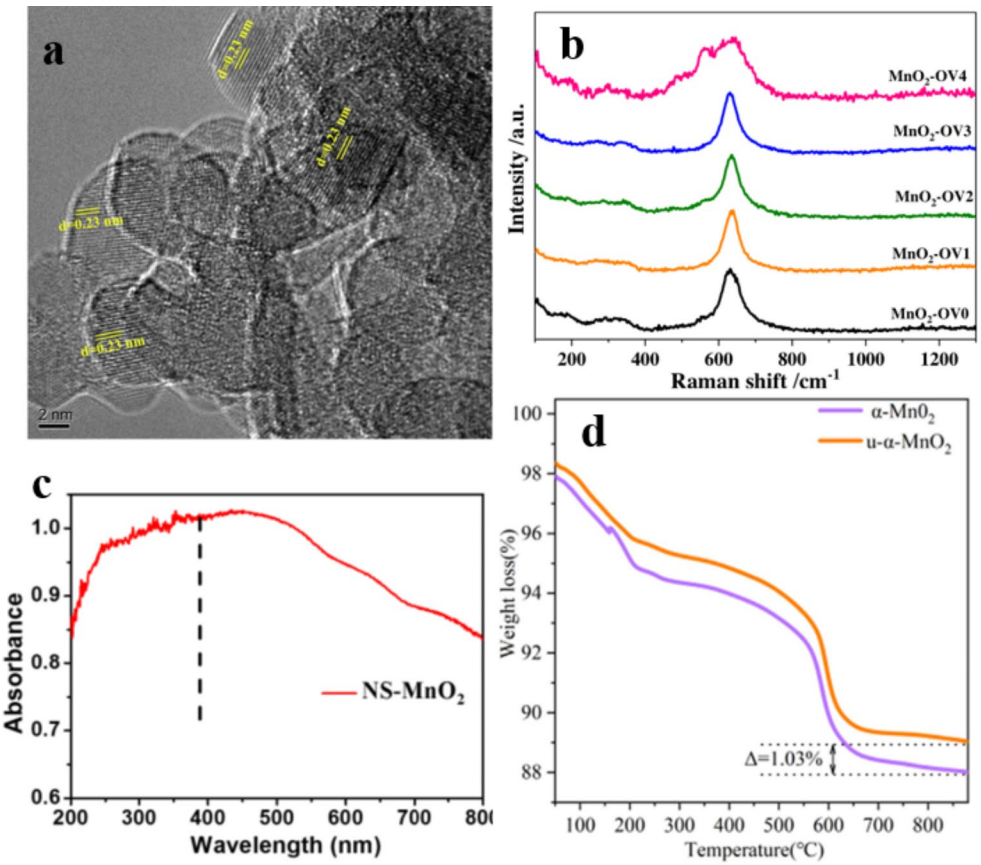

Fig. 9 (**a**) TEM image of nano-δ-MnO_2, (**b**) Raman spectra of the MnO_2 catalysts, (**c**) UV-vis diffuse reflectance spectrum of NS-MnO_2, (**d**) TG analysis curves of the a-MnO_2 and u-a-MnO_2 samples

[16]. The depth of Raman detection is about 10 nm, it always is used to characterize the exit of surface V_O.

4.2.3 UV-visible Diffuse Reflectance Spectrum (UV-vis)

The UV-visible diffuse reflectance spectrum (UV-vis) can also provide evidence for the presence of Mn^{3+} in MnO_2 (Fig. 9c). The peak at ≈380 nm is the characteristic peak of Mn^{3+} [9]. However, its penetration capability is weak and it can only detect the presence of surface Mn^{3+}, thus indirectly characterizing the presence of surface V_O.

4.2.4 Thermogravimetry(TG)

As shown in Fig. 9d [50], the weight loss of the u-a-MnO_2 sample is 1.03% less than that of the well-prepared a-MnO_2 sample. The results indicate that the repopulation of oxygen atoms at Vo during the thermal process suppressed the weight loss of the u-a-MnO_2 sample. Thus, the TG analysis confirmed the presence of V_O.

4.2.5 Other Characterization Methods

In addition, noise-filtered images, [34] H_2 programmed temperature rise reduction (H_2-TPR), O_2 programmed temperature rise desorption (O_2-TPD), [40] X-ray absorption fine structure (XAFS), and positron annihilation lifetime spectroscopy (PALS) are available for the qualitative characterization of catalyst surface or bulk phase V_O (Fig. 8d) [47].

5 Issues and Prospects

At present, the study of V_O in MnO_2 nanocatalysts has attracted much attention.

Surface V_O and bulk V_O contributions were found to improve the catalytic performance of the MnO_2 nano-catalyst together. The surface V_O, acting as active sites, will continuously switch the environmental O_2 into active oxygen species. While moderate bulk V_O will facilitate the separation of photon-induced electrons and holes and thus extend the lifetime of carriers. The variation of the band gap of MnO_2 depends strongly on the content of oxygen vacancies, and the removal of oxygen ions leads to additional spin-polarized vacancy states (thus further reducing the band gap), As the number of V_O increases, the interaction with Mn atoms disappears, and the lower-lying d orbitals fade away. The band gap broadening follows this. (Fig. 10).

However, the following important questions are still highly expected to be answered.

(1) It has been advocated that surface lattice oxygen is also involved in the catalytic reaction. While whether it was oxidated into oxygen species by V_O as surface-adsorbed O_2 has not been concluded.
(2) Whether the doping of other non-metallic elements such as F can also weaken the Mn-O bond to allow more easily escape of the lattice oxygen?
(3) As shown in Fig. 10, both bulk oxygen vacancies and surface oxygen vacancies can improve the catalytic activity of MnO_2 in different ways, and the simultaneous presence of both can increase the light absorption

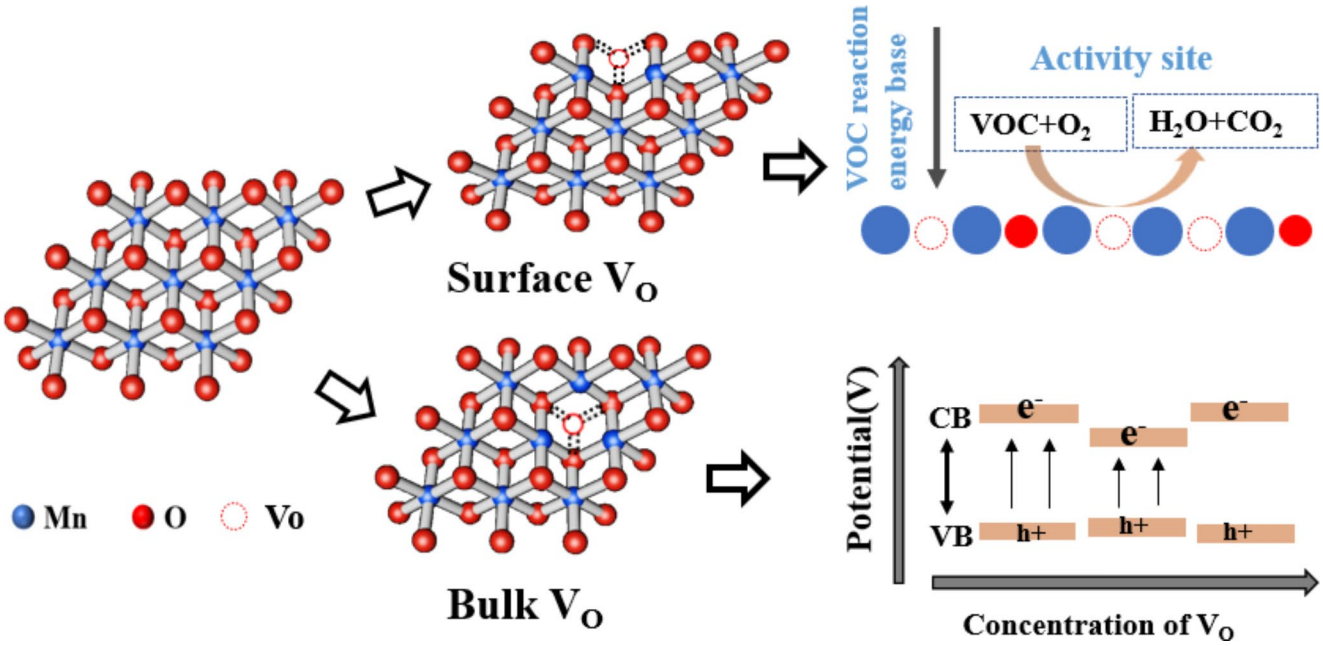

Fig. 10 The mechanism of action bulk and surface V_O

efficiency of MnO_2 while reducing the reaction energy base of VOC.

Acknowledgements This work is supported by the Department of Education of Guangdong Province (2019GZDXM006).

Author Contributions YaHui Zhou wrote the main manuscript text and others prepared Figs. 1, 2, 3, 4, 5, 6, 7 and 8. All authors reviewed the manuscript.

Declarations

Conflict of Interest No potential conflict of interest was reported by the author(s).

References

1. Guo Y, Wen M, Li G, An T (2021) Recent advances in VOC elimination by Catalytic Oxidation Technology onto various nanoparticles catalysts: a critical review. Appl Catal B 281:119447. https://doi.org/10.1016/j.aPcatb.2020.119447
2. Jeong GH, Sasikala SP, Yun T, Lee GY, Lee WJ, Kim SO (2020) Nanoscale Assembly of 2D materials for Energy and Environmental Applications. Adv Mater 32(35):1907006. https://doi.org/10.1002/adma.201907006
3. Wang J, Li J, Jiang C, Zhou P, Zhang P, Yu J (2017) The Effect of Manganese Vacancy in Birnessite-Type MnO_2 on Room-Temperature Oxidation of Formaldehyde in Air. *Applied Catalysis B: Environmental*, *204*, 147–155. DOI: https://doi.org/10.1016/j.apcatb.2016.11.036
4. Sekine Y, Fukuda M, Takao Y, Ozano T, Sakuramoto H, Wang KW (2011) Simultaneous removal of formaldehyde and benzene in indoor air with a combination of Sorption- and decomposition-type air filters. Environ Technol 32(16):1983–1989. https://doi.org/10.1080/09593330.2011.562924
5. Tian F-X, Li H, Zhu M, Tu W, Lin D, Han Y-F (2022) Effect of MnO_2 polymorphs' structure on low-temperature Catalytic Oxidation: crystalline controlled oxygen vacancy formation. ACS Appl Mater Interfaces 14(16):18525–18538. https://doi.org/10.1021/acsami.2c01727
6. Wang F, Dai H, Deng J, Bai G, Ji K, Liu Y (2012) Manganese oxides with Rod-, Wire-, Tube-, and Flower-Like Morphologies: highly effective catalysts for the removal of Toluene. Environ Sci Technol 46(7):4034–4041. https://doi.org/10.1021/es204038j
7. Zhang A, Gao R, Hu L, Zang X, Yang R, Wang S, Yao S, Yang Z, Hao H, Yan Y-M (2021) Rich Bulk Oxygen Vacancies-Engineered MnO_2 with enhanced charge transfer kinetics for Supercapacitor. Chem Eng J 417:129186. https://doi.org/10.1016/j.cej.2021.129186
8. Zhu G, Zhu J, Jiang W, Zhang Z, Wang J, Zhu Y, Zhang Q (2017) Surface Oxygen Vacancy Induced α-MnO_2 nanofiber for highly efficient ozone elimination. Appl Catal B 209:729–737. https://doi.org/10.1016/j.apcatb.2017.02.068
9. Zhao Y, Chang C, Teng F, Zhao Y, Chen G, Shi R, Waterhouse GIN, Huang W, Zhang T (2017) Defect-Engineered ultrathin δ-MnO_2 nanosheet arrays as bifunctional electrodes for efficient overall water splitting. Adv Energy Mater 7(18):1700005. https://doi.org/10.1002/aenm.201700005
10. Yang Y, Zhang S, Wang S, Zhang K, Wang H, Huang J, Deng S, Wang B, Wang Y, Yu G (2015) Ball Milling Synthesized MnO_x as Highly Active Catalyst for Gaseous POPs Removal: Significance of Mechanochemically Induced Oxygen Vacancies. Environ Sci Technol 49(7):4473–4480. https://doi.org/10.1021/es505232f
11. Li L, Feng X, Nie Y, Chen S, Shi F, Xiong K, Ding W, Qi X, Hu J, Wei Z et al (2015) Insight into the Effect of Oxygen Vacancy Concentration on the Catalytic performance of MnO_2. ACS Catal 5(8):4825–4832. https://doi.org/10.1021/acscatal.00320
12. Chen, L.; Liu, Y.; Fang, X.; Cheng, Y. Simple Strategy for the Construction of Oxygen Vacancies on α-MnO_2 Catalyst to Improve Toluene Catalytic Oxidation. *Journal of Hazardous Materials*, 2021, *409*, 125020. DOI: https://doi.org/10.1016/j.jhazmat.2020.125020
13. Schaub, R.; Thostrup, P.; Lopez, N.; Lægsgaard, E.; Stensgaard, I.; Nørskov, J.K.; Besenbacher, F. Oxygen Vacancies as Active Sites for Water Dissociation on Rutile TiO_2 (110). *Phys. Rev. Lett*, 2001, *87* (26), 266104. DOI: https://doi.org/10.1103/PhysRevLett.87.266104
14. Yang, W.; Zhu, Y.; You, F.; Yan, L.; Ma, Y.; Lu, C.; Gao, P.; Hao, Q.; Li, W.Insights into the Surface-Defect Dependence of Molecular Oxygen Activation over Birnessite-Type MnO_2. *Applied Catalysis B: Environmental*, 2018, *233*, 184–193. DOI: https://doi.org/10.1016/j.apcatb.2018.03.107.
15. Santos, V. P.; Pereira, M. F. R.; Órfão, J. J. M.; Figueiredo, J. L. The Role of Lattice Oxygen on the Activity of Manganese Oxides towards the Oxidation of Volatile Organic Compounds. *Applied Catalysis B: Environmental*, 2010, *99* (1–2), 353–363. DOI: https://doi.org/10.1016/j.apcatb.2010.07.007.
16. Dong, C.; Qu, Z.; Jiang, X.; Ren, Y. Tuning Oxygen Vacancy Concentration of MnO_2 through Metal Doping for Improved Toluene Oxidation. *Journal of Hazardous Materials*, 2020, *391*, 122181. DOI: https://doi.org/10.1016/j.jhazmat.2020.122181.
17. Cheng, F.; Zhang, T.; Zhang, Y.; Du, J.; Han, X.; Chen, J. Enhancing Electrocatalytic Oxygen Reduction on MnO_2 with Vacancies. *Angew. Chem. Int. Ed*, 2013, *52* (9), 2474–2477. DOI: https://doi.org/10.1002/anie.201208582.
18. Yang, R.; Peng, S.; Lan, B.; Sun, M.; Zhou, Z.; Sun, C.; Gao, Z.; Xing, G.; Yu,L. Oxygen Defect Engineering of B-MnO_2 Catalysts via Phase Transformation for Selective Catalytic Reduction of NO. *Small*, 2021, *17* (43), 2102408. DOI: https://doi.org/10.1002/smll.202102408.
19. Wang, Y.; Wu, J.; Wang, G.; Yang, D.; Ishihara, T.; Guo, L. Oxygen Vacancy Engineering in Fe Doped Akhtenskite-Type MnO_2 for Low-Temperature Toluene Oxidation. *Applied Catalysis B: Environmental*, 2021, *285*, 119873. DOI: https://doi.org/10.1016/j.apcatb.2020.119873.
20. Wang, Y.; Liu, K.; Wu, J.; Hu, Z.; Huang, L.; Zhou, J.; Ishihara, T.; Guo, L.Unveiling the Effects of Alkali Metal Ions Intercalated in Layered MnO_2 for Formaldehyde Catalytic Oxidation. *ACS Catal*, 2020, *10* (17), 10021–10031. DOI: https://doi.org/10.1021/acscatal.0c02310.
21. Ndayiragije, S.; Zhang, Y.; Zhou, Y.; Song, Z.; Wang, N.; Majima, T.; Zhu, L.Mechanochemically Tailoring Oxygen Vacancies of MnO_2 for Efficient Degradation of Tetrabromobisphenol A with Peroxymonosulfate. *Applied Catalysis B: Environmental*, 2022, *307*, 121168. DOI: https://doi.org/10.1016/j.apcatb.2022.121168.
22. Tang, Q.; Jiang, L.; Liu, J.; Wang, S.; Sun, G. Effect of Surface Manganese Valence of Manganese Oxides on the Activity of the Oxygen Reduction Reaction in Alkaline Media.*ACS Catal*, 2014, *4* (2), 457–463. DOI: https://doi.org/10.1021/cs400938s.
23. Saputra, E.; Muhammad, S.; Sun, H.; Ang, H.-M.; Tadé, M. O.; Wang, S. Manganese Oxides at the Different Oxidation States for Heterogeneous Activation of Peroxymonosulfate for Phenol Degradation in Aqueous Solutions. *Applied Catalysis B: Environmental*, 2013, *142–143*, 729–735. DOI: https://doi.org/10.1016/j.apcatb.2013.06.004.
24. Chen, J.; Tang, H.; Huang, M.; Yan, Y.; Zhang, J.; Liu, H.; Zhang, J.; Wang, G.;Wang, R. Surface Lattice Oxygen Activation by

Nitrogen-Doped Manganese Dioxide as an Effective and Longevous Catalyst for Indoor HCHO Decomposition. *ACS Appl Mater Inter*, 2021, *13* (23), 26960–26970. DOI: https://doi.org/10.1021/acsami.1c04369.

25. Do, S.-B.; Lee, S.-E.; Kim, T.-O. Oxidative Decomposition with PEG-MnO2 Catalyst for Removal of Formaldehyde: Chemical Aspects on HCHO Oxidation Mechanism. *Applied Surface Science*, 2022, *598*, 153773. DOI: https://doi.org/10.1016/j.apsusc.2022.153773
26. Ji, J.; Lu, X.; Chen, C.; He, M.; Huang, H. Potassium-Modulated δ-MnO_2 as Robust Catalysts for Formaldehyde Oxidation at Room Temperature. *Applied Catalysis B: Environmental*, 2020, *260*, 118210. DOI: https://doi.org/10.1016/j.apcatb.2019.118210.
27. Li, X.; Chen, M.; Li, G.; Wang, P. Constructing MnO_2 Alpha/Amorphous Heterophase Junction by Mechanochemically Induced Phase Transformation for Formaldehyde Oxidation. *Applied Surface Science*, 2022, *589*, 152855. DOI: https://doi.org/10.1016/j.apsusc.2022.152855.
28. Mang, C.; Luo, J.; Cao, P.; Zhang, X.; Rao, M.; Li, G.; Jiang, T. Importance of Water Content in Birnessite-Type MnO_2 Catalysts for HCHO Oxidation: Mechanistic Details and DFT Analysis. *Chemosphere*, 2022, *287*, 132293. DOI: https://doi.org/10.1016/j.chemosphere.2021.132293.
29. Rong, S.; Zhang, P.; Liu, F.; Yang, Y. Engineering Crystal Facet of α-MnO_2 Nanowire for Highly Efficient Catalytic Oxidation of Carcinogenic Airborne Formaldehyde.*ACS Catal*, 2018, *8* (4), 3435–3446. DOI: https://doi.org/10.1021/acscatal.8b00456.
30. Zhou, L.; Wang, C.; Li, Y.; Liu, X.; Deng, H.; Shan, W.; He, H. The Effect of Hydrogen Reduction of α-MnO_2 on Formaldehyde Oxidation: The Roles of Oxygen Vacancies. *Chinese Chem Lett*, 2022, S1001841722006039. DOI: https://doi.org/10.1016/j.cclet.2022.06.028.
31. Zhu, L.; Wang, J.; Rong, S.; Wang, H.; Zhang, P. Cerium Modified Birnessite-Type MnO_2 for Gaseous Formaldehyde Oxidation at Low Temperature. *Applied Catalysis B: Environmental*, 2017, *211*, 212–221. DOI: https://doi.org/10.1016/j.apcatb.2017.04.025.
32. He, T.; Shao, D.; Zeng, X.; Rong, S. Harvesting the Vibration Energy of α-MnO_2 Nanostructures for Complete Catalytic Oxidation of Carcinogenic Airborne Formaldehyde at Ambient Temperature. *Chemosphere*, 2020, *261*, 127778. DOI: https://doi.org/10.1016/j.chemosphere.2020.127778.
33. Ye, Z.; Li, T.; Ma, G.; Dong, Y.; Zhou, X. Metal-Ion (Fe, V, Co, and Ni)-Doped MnO_2 Ultrathin Nanosheets Supported on Carbon Fiber Paper for the Oxygen Evolution Reaction.*Adv. Funct. Mater*, 2017, *27* (44), 1704083. DOI: https://doi.org/10.1002/adfm.201704083.
34. Chu, K.; Liu, Y.; Cheng, Y.; Li, Q. Synergistic Boron-Dopants and Boron-Induced Oxygen Vacancies in MnO_2 Nanosheets to Promote Electrocatalytic Nitrogen Reduction. *J. Mater. Chem. A*, 2020, *8* (10), 5200–5208. DOI: https://doi.org/10.1039/D0TA00220H.
35. He, T.; Zeng, X.; Rong, S. The Controllable Synthesis of Substitutional and Interstitial Nitrogen-Doped Manganese Dioxide: The Effects of Doping Sites on Enhancing the Catalytic Activity. *J. Mater. Chem. A*, 2020, *8* (17), 8383–8396. DOI: https://doi.org/10.1039/D0TA01346C.
36. Wang, J.; Li, J.; Zhang, P.; Zhang, G. Understanding the "Seesaw Effect" of Interlayered K^+ with Different Structure in Manganese Oxides for the Enhanced Formaldehyde Oxidation.*Applied Catalysis B: Environmental*, 2018, *224*, 863–870. DOI: https://doi.org/10.1016/j.apcatb.2017.11.019.
37. Choi, Y.; Lim, D.; Oh, E.; Lim, C.; Baeck, S.-H. Effect of Proton Irradiation on Electrocatalytic Properties of MnO_2 for Oxygen Reduction Reaction. *J. Mater. Chem. A*, 2019, *7* (19), 11659–11664. DOI: https://doi.org/10.1039/C9TA03879E.
38. Luo, J.; Zhang, Q.; Garcia-Martinez, J.; Suib, S. L. Adsorptive, and Acidic Properties,Reversible Lattice Oxygen Evolution, and Catalytic Mechanism of Cryptomelane-Type Manganese Oxides as Oxidation Catalysts. *J. Am. Chem. Soc*, 2008, *130* (10), 3198–3207. DOI: https://doi.org/10.1021/ja077706e.
39. James, S. L.; Adams, C. J.; Bolm, C.; Braga, D.; Collier, P.; Friščić, T.; Grepioni,F.; Harris, K. D. M.; Hyett, G.; Jones, W.; et al. Mechanochemistry: Opportunities for New and Cleaner Synthesis. *Chem. Soc. Rev*, 2012, *41* (1), 413–447. DOI: https://doi.org/10.1039/C1CS15171A.
40. Mo, S.; Zhang, Q.; Li, J.; Sun, Y.; Ren, Q.; Zou, S.; Zhang, Q.; Lu, J.; Fu, M.;Mo, D.; et al. Highly Efficient Mesoporous MnO_2 Catalysts for the Total Toluene Oxidation: Oxygen-Vacancy Defect Engineering and Involved Intermediates Using in Situ DRIFTS. *Applied Catalysis B: Environmental*, 2020, *264*, 118464. DOI: https://doi.org/10.1016/j.apcatb.2019.118464.
41. Huang, Y.; Liu, Y.; Wang, W.; Chen, M.; Li, H.; Lee, S.; Ho, W.; Huang, T.; Cao,J. Oxygen Vacancy–Engineered δ-MnO/Activated Carbon for Room-Temperature Catalytic Oxidation of Formaldehyde. *Applied Catalysis B: Environmental*, 2020, *278*, 119294. DOI: https://doi.org/10.1016/j.apcatb.2020.119294.
42. Yan, L.; Shen, C.; Niu, L.; Liu, M.; Lin, J.; Chen, T.; Gong, Y.; Li, C.; Liu,X.; Xu, S. Experimental and Theoretical Investigation of the Effect of Oxygen Vacancies on the Electronic Structure and Pseudocapacitance of MnO_2. *ChemSusChem*, 2019, *12* (15), 3571–3581. DOI: https://doi.org/10.1002/cssc.201901015.
43. Liu, F.; Rong, S.; Zhang, P.; Gao, L. One-Step Synthesis of Nanocarbon-Decorated MnO_2 with Superior Activity for Indoor Formaldehyde Removal at Room Temperature. *Applied Catalysis B: Environmental*, 2018, *235*, 158–167. DOI: https://doi.org/10.1016/j.apcatb.2018.04.078.
44. Yi, H.; Wang, Y.; Diao, L.; Xin, Y.; Chai, C.; Cui, D.; Ma, D. Ultrasonic Treatment Enhances the Formation of Oxygen Vacancies and Trivalent Manganese on α-MnO_2 Surfaces: Mechanism and Application. *Journal of Colloid and Interface Science*, 2022, *626*, 629–638. DOI: https://doi.org/10.1016/j.jcis.2022.06.144.
45. Cui, P.; Zhang, Y.; Cao, Z.; Liu, Y.; Sun, Z.; Cheng, S.; Wu, Y.; Fu, J.; Xie,E. Plasma-Assisted Lattice Oxygen Vacancies Engineering Recipe for High-Performing Supercapacitors in a Model of Birnessite-MnO_2. *Chemical Engineering Journal*, 2021, *412*, 128676. DOI: https://doi.org/10.1016/j.cej.2021.128676.
46. Zhou, Y.; Zhou, Z.; Hu, L.; Tian, R.; Wang, Y.; Arandiyan, H.; Chen, F.; Li, M.;Wan, T.; Han, Z.; et al. A Facile Approach to Tailor Electrocatalytic Properties of MnO_2 through Tuning Phase Transition, Surface Morphology, and Band Structure. *Chemical Engineering Journal*, 2022, *438*, 135561. DOI: https://doi.org/10.1016/j.cej.2022.135561.
47. Ye, K.; Li, K.; Lu, Y.; Guo, Z.; Ni, N.; Liu, H.; Huang, Y.; Ji, H.; Wang, P.An Overview of Advanced Methods for the Characterization of Oxygen Vacancies in Materials.*TrAC Trends in Analytical Chemistry*, 2019, *116*, 102–108. DOI: https://doi.org/10.1016/j.trac.2019.05.002.
48. Jiang, Y.-F.; Jiang, N.; Liang, K.; Yuan, C.-Z.; Fang, X.-X.; Xu, A.-W. A Simple and General Route to Prepare Functional Mesoporous Double-Metal Oxy(Hydroxide). *J. Mater. Chem. A*, 2019, *7* (13), 7932–7938. DOI: https://doi.org/10.1039/C8TA10719J.
49. Wang, Y.; Cai, J.; Wu, M.; Chen, J.; Zhao, W.; Tian, Y.; Ding, T.; Zhang, J.;Jiang, Z.; Li, X. Rational Construction of Oxygen Vacancies onto Tungsten Trioxide to Improve Visible Light Photocatalytic Water Oxidation Reaction. *Applied Catalysis B: Environmental*, 2018, *239*, 398–407. DOI: https://doi.org/10.1016/j.apcatb.2018.08.029.
50. Chen, J.; Chen, X.; Yan, D.; Jiang, M.; Xu, W.; Yu, H.; Jia, H. A Facile Strategy of Enhancing Interaction between Cerium and Manganese Oxides for Catalytic Removal of Gaseous Organic

Contaminants. *Applied Catalysis B: Environmental*, 2019, *250*, 396–407. DOI: https://doi.org/10.1016/j.apcatb.2019.03.042.

51. Ji, J.; Lu, X.; Chen, C.; He, M.; Huang, H. Potassium-Modulated δ-MnO_2 as Robust Catalysts for Formaldehyde Oxidation at Room Temperature. *Applied Catalysis B: Environmental*, 2020, *260*, 118210. DOI: https://doi.org/10.1016/j.apcatb.2019.118210.
52. Fang, G.; Zhu, C.; Chen, M.; Zhou, J.; Tang, B.; Cao, X.; Zheng, X.; Pan, A.;Liang, S. Suppressing Manganese Dissolution in Potassium Manganate with Rich Oxygen Defects Engaged High-Energy-Density and Durable Aqueous Zinc-Ion Battery. *Adv. Funct. Mater*, 2019, *29* (15), 1808375. DOI: https://doi.org/10.1002/adfm.201808375.
53. Yang, R.; Peng, S.; Lan, B.; Sun, M.; Zhou, Z.; Sun, C.; Gao, Z.; Xing, G.; Yu,L. Oxygen Defect Engineering of Beta-MnO_2 Catalysts via Phase Transformation for Selective Catalytic Reduction of NO. *Small*, 2021, *17* (43), 2102408. DOI: https://doi.org/10.1002/smll.202102408.